Carbohydrate Polymers 111 (2014) 722–728

Contents lists available at ScienceDirect

Carbohydrate Polymers

journal homepage: www.elsevier.com/locate/carbpol

Evolution of morphology of bacterial cellulose scaffolds during early culture

Honglin Luo [a], Jing Zhang [a], Guangyao Xiong [b], Yizao Wan [a,*]

[a] School of Materials Science and Engineering, Tianjin University, Tianjin Key Laboratory of Composite and Functional Materials, Tianjin 300072, PR China
[b] School of Mechanical and Electrical Engineering, East China Jiaotong University, Nanchang 330013, Jiangxi, PR China

ARTICLE INFO

Article history:
Received 28 November 2013
Received in revised form 3 March 2014
Accepted 28 April 2014
Available online 6 May 2014

Keywords:
Bacterial cellulose
Tissue engineering scaffold
Morphology
Hydroxyapatite

ABSTRACT

Morphological characteristics of a fibrous tissue engineering (TE) scaffold are key parameters affecting cell behavior. However, no study regarding the evolution of morphology of bacterial cellulose (BC) scaffolds during the culture process has been reported to date. In this work, BC scaffolds cultured for different times starting from 0.5 h were characterized. The results demonstrated that the formation of an integrated scaffold and its 3D network structure, porosity, fiber diameter, light transmittance, and the morphology of hydroxyapatite (HAp)-deposited BC scaffolds changed with culture time. However, the surface and crystal structure of BC fibers did not change with culture time and no difference was found in the crystal structure of HAp deposited on BC templates regardless of BC culture time. The findings presented herein suggest that proper selection of culture time can potentially enhance the biological function of BC TE scaffold by optimizing its morphological characteristics.

1. Introduction

Bacterial cellulose (BC) is a pure form of extracellular cellulose secreted by many species of bacteria such as *Acetobacter xylinum* (Petersen & Gatenholm, 2011). Due to its outstanding properties including fine three-dimensional (3D) porous network structure, high mechanical properties, high water holding capacity, and so on (Chang, Chen, Lin, & Chen, 2012), BC shows a wide variety of applications in food, paper and textile industry, especially in biomedical fields such as wound dressings (Fu et al., 2012; Lin, Lien, Yeh, Yu, & Hsu, 2013; Ul-Islam, Khan, Khattak, & Park, 2013), artificial blood vessels (Andrade et al., 2013; Berti et al., 2011; Wan et al., 2011), and in particular nanofibrous scaffolds for tissue engineering (TE) (Dugan, Gough, & Eichhorn, 2013; Saska et al., 2012; Sundberg et al., 2012; Svensson et al., 2005; Wang, Gao, Zhang, & Wan, 2010; Wang et al., 2013). It has been well documented that porosity, fiber density (Berti, Rambo, Dias, & Porto, 2013; Petersen & Gatenholm, 2011), fiber diameter (Bashur, Dahlgren, & Goldstein, 2006), and even thickness and light transmittance (in the case of skin and cornea TE) of a scaffold have a significant impact on cell-material interaction and thus cell behavior. In addition, BC has also been widely considered as an ideal template material for the deposition of inorganic particles such as hydroxyapatite (HAp) (Wan et al., 2006), $CaCO_3$ (Liu, Ma, Zhou, Pei, & Yin, 2013), SiO_2 (Barud et al., 2008), Cu_2O (Liu et al., 2011), and ZnO (Costa, Gonçalves, Zaghete, Mazon, & Nogueira, 2013). Among these, HAp is considered the most important material in biomedical field since it is a major and essential component of normal bone and teeth and HAp/BC nanocomposites are believed to be a promising scaffold for bone TE (Wan et al., 2006). In this case, the surface structure of BC templates can greatly affect the morphology and structure of deposited particles (Costa et al., 2013; Liu et al., 2011; Wan et al., 2006). However, how the morphology of BC templates affects the characteristics of deposited products as well as how the culture time of BC affects the morphological properties of BC pellicles are unclear.

The studies on the applications of BC have been quite extensive but BC was usually cultured for 7 days or longer. To date, there is no report on the control of morphology (including fiber diameter, porosity, fiber network structure) and surface and crystal structure of BC during its growth process, in particular during its initial growth process within 7 days. For instance, a relevant study performed by Sheykhnazari, Tabarsa, Ashori, Shakeri, and Golalipour (2011) confirmed the effect of culture time on the structural characteristics of BC. However, this research focused on the BC cultured starting from day 7 and the sampling times are sparse (7, 14 and 21 days). Very recently, Zhang investigated the development of BC fibrils and the formation of BC bundles/ribbons along

* Corresponding author. Tel.: +86 22 2740 3045; fax: +86 22 2740 4724.
E-mail addresses: hlluo@tju.edu.cn, yzwantju@126.com, yzwan@tju.edu.cn (Y. Wan).

http://dx.doi.org/10.1016/j.carbpol.2014.04.097
0144-8617/

with the biosynthesis time ranging from 2 h to 48 h using atomic force microscopy and found that the length and diameter of single BC fibril changed with biosynthesis time (Zhang, 2013). In fact, the biosynthesis mechanism and the formation of BC nanofibers were extensively investigated as early as 1970s (Brown, Willison, & Richardson, 1976). However, the control of morphology of BC pellicles and its feasibility as TE scaffolds during the early culture process still remain ambiguous.

Therefore, the aim of this work was to investigate the evolution of morphology of BC pellicles during its whole culture process starting from as early as 0.5 h to 14 days in an attempt to suitably control the BC scaffolds for various TE applications. To this end, the BC samples obtained at different culture times were characterized and further used as templates for HAp deposition. It is believed that this research could enable us to optimize the culture time of BC scaffolds based upon the requirements of various TE applications.

2. Experimental

2.1. Preparation of BC

A. xylinum X-2 was used in this work to prepare BC samples. The detailed procedures and treatment methods were reported in our previous work (Hong et al., 2006; Wan et al., 2006). Typically, the culture medium of BC containing 2.5% glucose (Amerso), 0.75% yeast (Oxoid), 1% tryptone (Oxoid) and 1% Na_2HPO_4 (Alfa Aesar) was prepared and the pH was adjusted to 4.5 by acetic acid (Acros), followed by sterilizing at 115 °C for half an hour. Then the bacteria strain was incubated statically in the culture medium for different lengths of time. At given culture time intervals, the BC samples were collected and purified in NaOH solution and deionized water. The obtained BC samples were stored in distilled water until required.

2.2. Deposition of HAp on BC cultured for different times

The deposition of HAp on BC cultured for different times was conducted as described previously (Hong et al., 2006; Wan et al., 2006). Briefly, all purified BC samples were phosphorylated first and immersed in a 0.1 M $CaCl_2$ (Acros) solution at 37 °C for 3 days prior to biomineralization. The $CaCl_2$ solution was renewed every 24 h. Then the treated BC samples were immersed in a 1.5 SBF (1.5 times simulated body fluid solution) at 37 °C for 7 days and the SBF solution was replaced every day. Finally, the HAp-deposited BC (namely BC/HAp) samples were rinsed with deionized water and freeze-dried.

2.3. Characterizations

The thickness of BC pellicles was measured by a vernier caliper at predetermined time intervals and the growth rate of BC hydrogel was expressed as thickness increase divided by time interval. The photographs of early cultured BC samples in deionized water were taken by digital camera (Canon PowerShot A800). The BC samples cultured within 15 h were air-dried at 60 °C for 8 h and the BC samples cultured after 15 h and all BC/HAp samples were freeze-dried for 48 h. For SEM observation, the samples were sputtered with gold and were evaluated by a field-emission scanning electron microscope (FE-SEM, FEI, Nanosem 430). The transmittance spectra of BC cultured for different times were recorded using a TU1810PC spectrophotometer (Beijing Purkinje General Instrument Co.). XRD was carried out by a Rigaku D/max 2500 to examine the crystalline structure. The range of scanning was from 1 to 60° at a speed of 0.02°/s. The surface properties of BC and BC/HAp samples were investigated using a Fourier transform infrared spectrometer (FTIR, Bio-Rad FTS 6000). The fiber diameter of BC was measured from SEM images. From each image, at least 100 (unless otherwise indicated) different fiber segments were randomly selected and their diameters were measured to generate an average fiber diameter, as described in the literature (Bhattarai, Edmondson, Veiseh, Matsen, & Zhang, 2005).

2.4. Porosity measurement

The porosity of BC scaffolds was measured by water displacement method at room temperature (Nge, Nogi, Yano, & Sugiyama, 2010; Sionkowska & Kozłowska, 2013; Tang, Jia, Jia, & Yang, 2010). Briefly, a water-impregnated BC sample with a known weight (W_1) was immersed in a graduated cylinder containing a known volume (V_1) of water for 10 min. The total volume of water and the water-impregnated BC sample was recorded as V_2. The volume difference ($V_2 - V_1$) represented the total volume of the BC sample (including the volume of BC skeleton and void). Then the water-impregnated BC sample was collected and dried in an oven at 70 °C. After complete drying, the weight of BC was measured (W_2). Thus the porosity of BC (P) can be calculated as follows:

$$P = \frac{(W_1 - W_2)/\rho}{(V_2 - V_1)} \quad (1)$$

where ρ denotes the density of water at room temperature. The values were expressed as mean ± SD ($n = 3$).

3. Results and discussions

3.1. Morphology of BC harvested at different time points

It has been well documented that the biosynthesis of BC is a multistep process that involves two main mechanisms: the synthesis of uridine diphosphoglucose (UDPGIc), followed by the polymerization of glucose into long and unbranched chains (the β-1,4-glucan chains) (Brown, 1987; Ross, Mayer, & Benziman, 1991). In this work, the focus was laid on the morphology of BC pellicles during the early growth process. Fig. 1 presents the morphology of BC fibrils synthesized by *A. xylinum* at the very first 3-h culture starting from 0.5 h. It was found that, at the beginning of culture, there were a large number of rodlike *A. xylinum* strains in the medium with an average length of 1.6 μm (Fig. 1a). Fig. 1b shows that no microfibril was extruded from the cell in the first 0.5 h. Zhang (2013) reported that single BC microfibrils with an average diameter of 5.8 nm were biosynthesized and microfibrils also began to bind with each other forming bundles after the first 2-h incubation. However, we found that a few fibrils with a diameter of 37 nm (averaged from 20 fibrils) were observed (Fig. 1c) as the culture time reached 1 h. Fig. 1d shows that two fibrils were assembled together forming a bigger fibril with an increased diameter of 90 nm (averaged from 20 fibrils). Therefore, it is inferred that the fibrils can be biosynthesized within the first 1-h incubation under the current culture conditions, and part of them began to bind with each other forming bigger bundles, which is inconsistent with previous finding by Brown et al. (1976) who declared that the single microfibril of BC could bind with each other and form a bundle after 24–48 h. Fig. 1e shows a larger fibril with a diameter of 102 nm (averaged from 30 fibrils) indicating a successive increase in diameter (due to fibril binding). As the culture time extended to 3 h, plenty of fibrils were formed (Fig. 1f). However, no floating pellicle could be observed until 6-h incubation.

Fig. 2 presents macrophotographs of the flocculent floating BC which was incubated for different lengths of time ranging from 6 to 12 h. Notably, after 6 to 12-h incubation, fibrils intertwined with each other forming a flocculent mesh and the amount of BC pellicles increased with culture time. However, integrated macroscopic BC

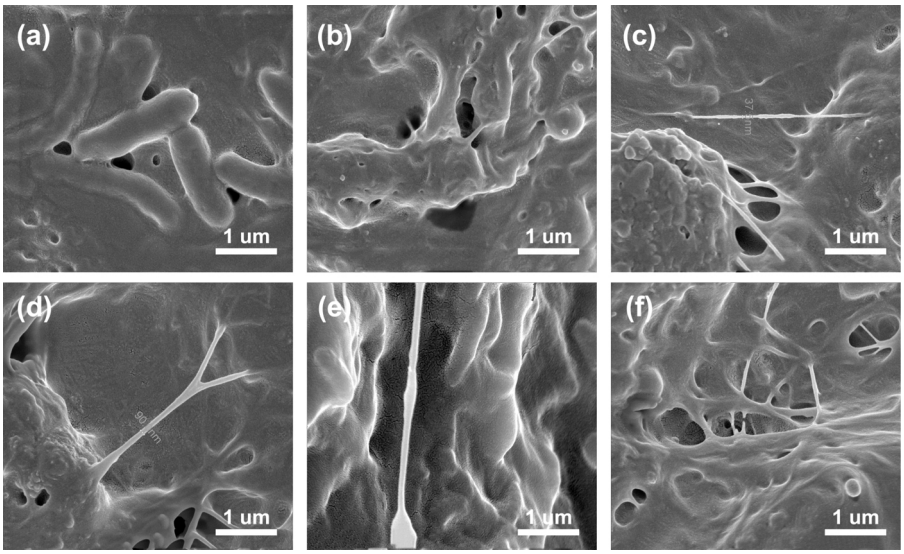

Fig. 1. FE-SEM images of BC samples prepared within 3 h (a) 0 h, (b) 0.5 h, (c) 1 h, (d) 1.5 h, (e) 2 h, and (f) 3 h.

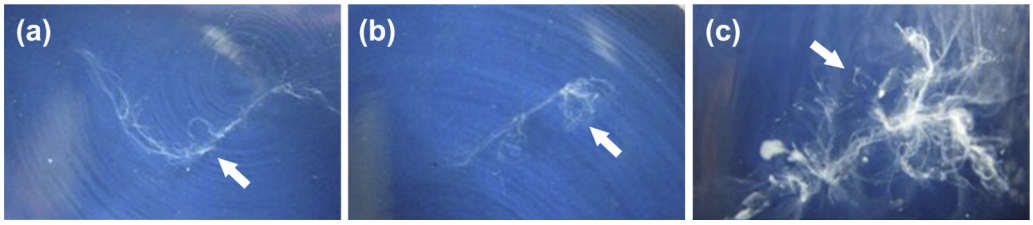

Fig. 2. Photographs of BC synthesized after (a) 6 h, (b) 8 h, and (c) 12 h.

films were not formed within the first 12-h growth. This indicates that 12 h is too short to create a practical BC scaffold.

Fig. 3 presents the SEM images of BC films obtained at culture time from 15 h to 14 days. In order to maintain the original structure of BC pellicles, these samples were freeze dried before SEM observation. Fig. 3a demonstrates that, at 15-h culture time, BC fibers were distributed unevenly and several fiber-depleted zones were observed (as marked by circles). This uneven distibution of BC fibers was caused by the freeze–drying due to the small average thickness (0.7 mm) and the observed rugged surface of BC pellicles during the first 15-h culture. The uneven distribution of BC fibers is not benifical to cell behavior. As the incubation time prolonged to 1 to 3 days (Fig. 3b–d), the distribution of BC fibers became uniform. Furthermore, an obvious 3D porous network structure started to form when the culture time reached 5 days or longer (insets in Fig. 3e–h), suggesting a complete 3D scaffold (in freeze dried state) was obtained. Therefore, to form a homogeneous BC thin film that can be used as a practical TE scaffold, the minimum culture time should be 24 h. This thin BC film (2D scaffold) in never-dried state (<1 mm in thickness) might be used for cornea TE. However,

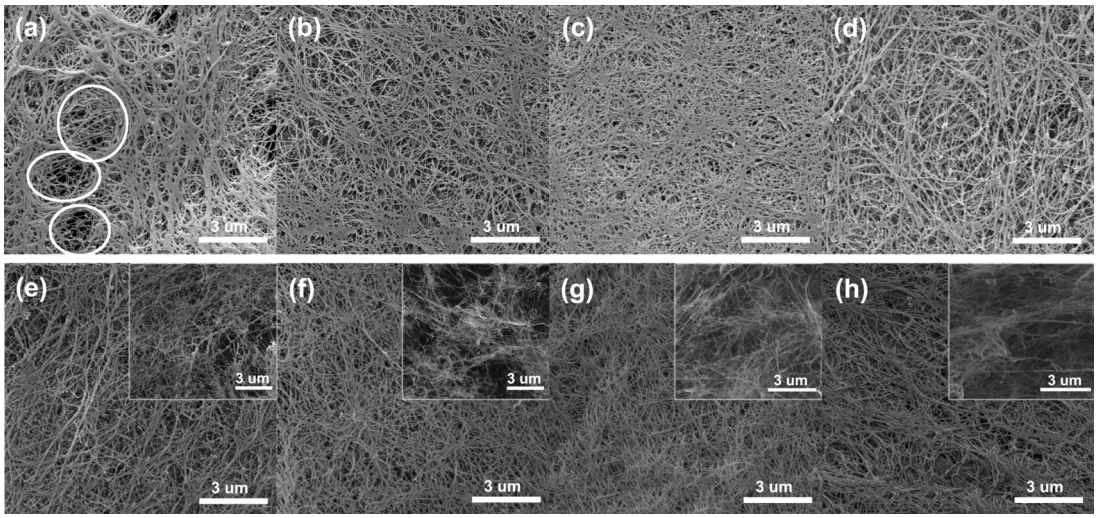

Fig. 3. SEM images of BC obtained after (a) 15 h, (b) 1 d, (c) 2 d, (d) 3 d, (e) 5 d, (f) 7 d, (g) 10 d, and (h) 14 d (insets showing the cross-sectional SEM images of corresponding BC samples).

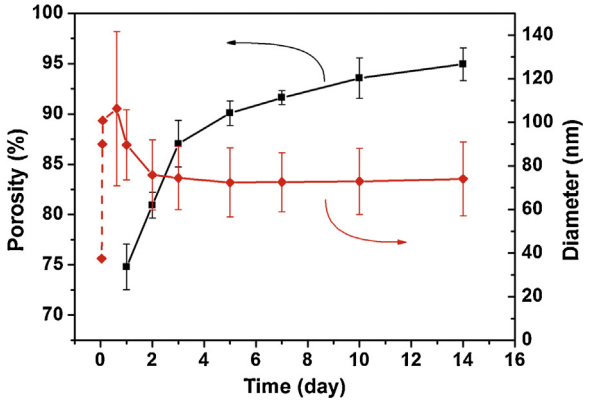

Fig. 4. Changes of porosity (a) and fiber diameter (b) as a function of BC culture time.

longer culture time (≥5days) is needed to obtain a complete 3D scaffold (>3 mm in freeze dried state). Notably, the 3D porous network structure was relatively stable and large amounts of pores were present inside the pellicles, which endowed themselves with excellent permeability. The stable fiber network structure is due to the fact that BC bundles and ribbons were formed through simple binding of single fibrils and twisting of fibrils (Zhang, 2013), both of which promoted the formation of structurally stable network of BC fibers.

Porosity measurement result (Fig. 4) reveals that the porosity increased markedly during the culture time of 1 to 3 days but the rate of increase subsequently slowed down. At 14-day culture, the porosity reached a maximum value of 95%. Diameter measurement result (Fig. 4) shows that the diameter of BC fibers experienced an increase during the first 24 h, followed by a slight decrease from 1 to 2 days, and subsequently plateaued to a relatively stable value of 72 nm. These results indicate that a suitable culture time should be selected for a specific TE application since porosity and fiber diameter determine cell behavior (Bashur et al., 2006; Berti et al., 2013). The observed variation in fiber diameter is probably related to the degree of clustering on the enzymatic and cytostructural level (Ross et al., 1991). However, the exact mechanism is still unclear since many aspects surrounding the nature of the biosynthetic machinery remain unsolved (Ross et al., 1991).

Previous work has confirmed that BC is a promising TE scaffold for cornea and skin (Fu, Zhou, Zhang, & Yang, 2013; Wang et al., 2010) where light transmittance and/or thickness are critical parameters. Fig. 5 shows the changes of light transmittance and thickness of BC films with the culture time. Note that the BC films (in wet state) maintained high transparency during their early growth within 24 h (Fig. 5a and b). As the incubation time further increased, the light transmittance displayed a rapid decrease from day 1 to day 5 and subsequently reached a plateau. Fig. 5b reveals that, for a cornea TE scaffold, the culture time should be 24 h or less since the percentage transmission should be at least 80% (at 450 nm) (Beems & Van Best, 1990). By combining Fig. 5b with Fig. 4, the optimal culture time should be 24 h in order to meet the requirements for both integrated structure and light transmittance. It is noted that the evolution of transparency of BC films was consistent with the change in their thickness shown in Fig. 5c. As can be seen from Fig. 5c, the growth of BC pellicles could be divided into three stages and the growth data at these three stages could be fitted into three linear plots (Iguchi, Yamanaka, & Budhiono, 2000; Yamanaka et al., 1989), which suggests that the growth of BC at each stage showed first-order kinetics. Note that the growth rate of the second stage (15 h to 5 days) was 1.82 mm/d, which was about 2.3 and 2.5 times that of the first (0 to 15 h) and third stages (5 to 14 days), respectively. The change of BC growth rate could be

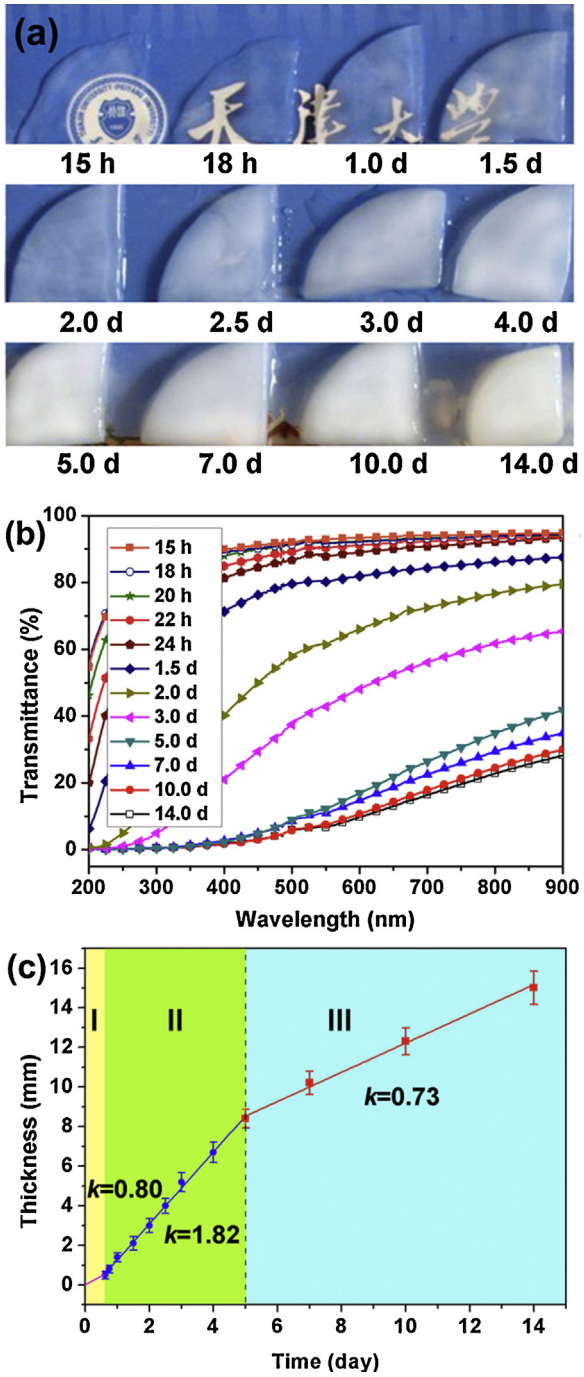

Fig. 5. Photographs (a), light transmittance (b), and thickness (c) of BC films cultured for different times.

explained as follows. At the first stage of BC growth, though the nutrient in the culture medium was adequate, the population of *A. xylinum* strains was very small, and thus the BC pellicles grew slowly. At the second stage, not only could the culture medium provide adequate nutrient, but also the bacteria population was significantly increased due to the rapid multiplication. Therefore, a high growth rate of BC pellicles was achieved. As the culture time increased to 5 days, most nutrients in the medium were consumed and the increase of BC pellicle thickness may also have a negative impact on the oxygen supply for *A. xylinum* strains, suppressing the formation of BC fibrils. Additionally, it was believed that, during the incubation process, *A. xylinum* strains would actively and continuously convert glucose into gluconic acid. This process lowered the

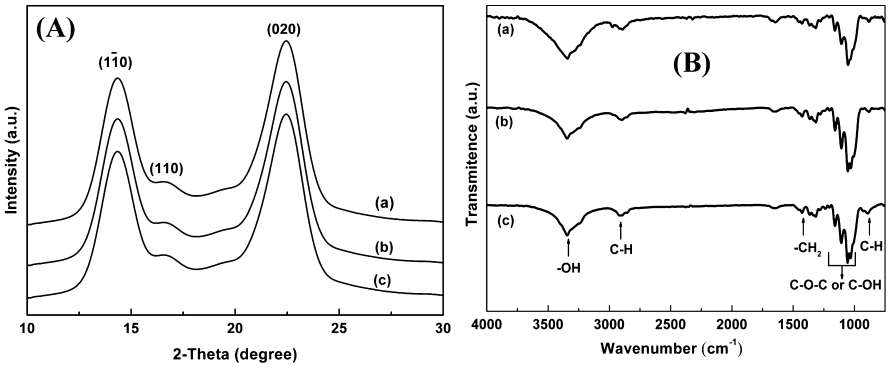

Fig. 6. XRD (A) and FTIR (B) patterns of BC at different culture times (a) 4 h, (b) 15 h, and (c) 5 d.

pH of the medium to suboptimal levels for *A. xylinum* growth and BC biosynthesis (Vandamme, De Baets, Vanbaelen, Joris, & De Wulf, 1998).

3.2. Structure of BC harvested at different time points

In addition to morphological characteristics, we also evaluated the surface and crystal structure stability of BC during its growth process. Fig. 6 shows the XRD and FTIR spectra of BC samples collected at three different culture times (4 h, 15 h and 5 days). Fig. 6A reveals that no difference can be detected among these three spectra which showed three characteristic peaks located at 14.8, 16.6, and 22.4°, corresponding to (1 $\bar{1}$ 0), (1 1 0), and (0 2 0) diffraction of cellulose I, respectively (Watanabe, Tabuchi, Morinaga, & Yoshinaga, 1998). Moreover, these three BC samples had an identical crystallinity index (89%) which was calculated according to the method reported by Sottys, Lisowski, and Knapczyk (1984).

Fig. 6B reveals that the three BC samples harvested at 4 h, 15 h, and 5 days had identical FTIR spectra. These FTIR patterns were typical spectra of BC where the absorption band assigned to the hydroxyl group and hydrogen bond was observed at 3200–3500 cm^{-1} and were consistent with our previous findings for 7-day cultured BC (Wan et al., 2006) and those reported in the literature (Kim, Nishiyama, & Kuga, 2002).

XRD and FTIR findings indicate that the crystal structure and surface chemistry of BC remained unchanged irrespective of culture time, which is beneficial to the potential applications of early grown BC in various TE applications as a potential substitute for long-time cultured BC at a reduced time and cost.

3.3. Morphology of HAp deposited on BC cultured at different times

The studies on biomineralization can not only help understand the process happened in vivo, but also find a biomimetic route to develop man-made mineralized nanofibers for bone TE scaffolds. In this work, the influence of BC morphology on the deposition of HAp on BC (i.e. biomineralization) was investigated. Fig. 7 displays the FE-SEM images of BC/HAp nanocomposites prepared by using BC templates cultured for different lengths of time. SEM observation reveals that all the surfaces of BC fibers on the surface layer were densely deposited by HAp particles. Obviously, the distribution and morphology of HAp particles did not present apparent difference among different BC templates used. However, the insets in Fig. 7

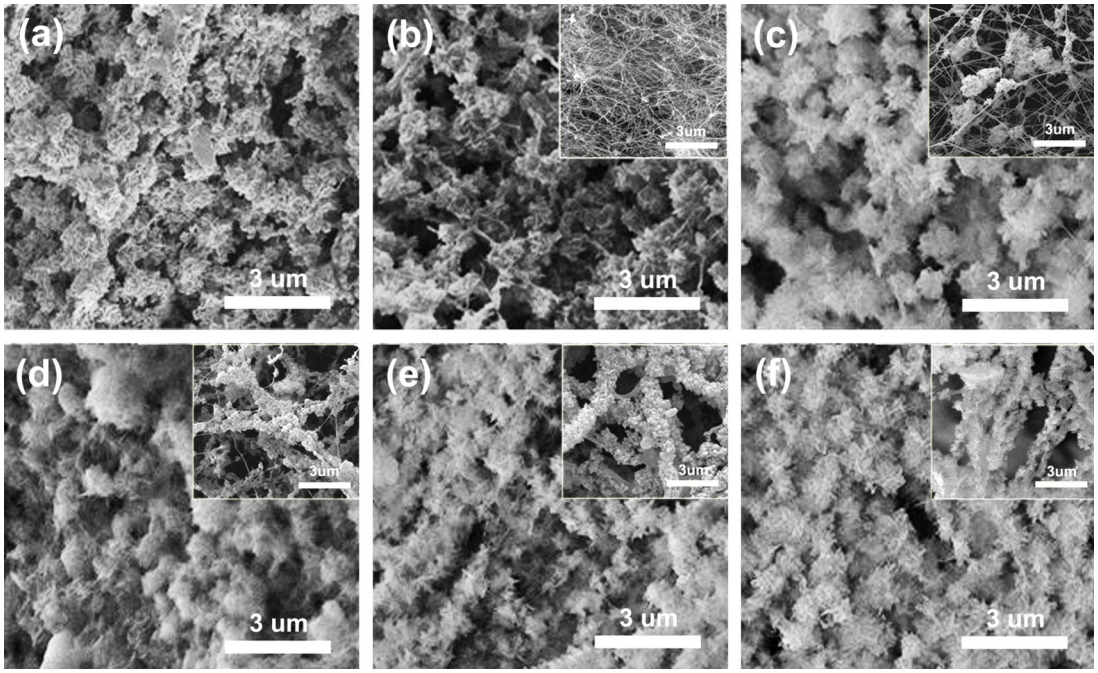

Fig. 7. FE-SEM images of BC/HAp samples with BC templates cultured for different times (a) 18 h, (b) 1 d, (c) 3 d, (d) 5 d, (e) 7 d, and (f) 10 d (insets showing the cross-sectional SEM images of corresponding BC/HAp samples).

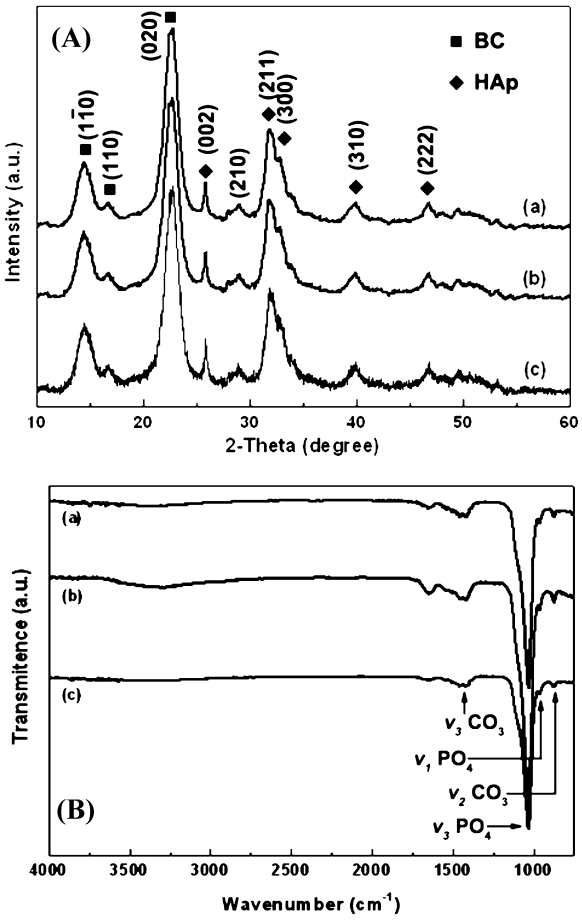

Fig. 8. XRD (A) and FTIR (B) patterns of various BC/HAp samples with BC templates cultured for different times (a) 1 d, (b) 5 d, and (c) 10 d.

evidenced the difference in the distribution of HAp particles on the cross-sections of corresponding BC templates. The inset in Fig. 7b reveals that sparsely distributed HAp particles were found on the fibers inside BC membranes. This could be attributed to the tight network structure of BC membranes that hindered the transportation of ions from 1.5 SBF solution to the inside of BC membranes, agreeing well with the porosity result. More and more HAp particles were observed on the fibrils inside BC membranes when BC membranes cultured at longer time were used as templates (insets of Fig. 7c–f), and finally, all the BC fibrils inside BC membranes were fully coated by HAp particles as shown in the insets of Fig. 7e and f, which is consistent with our previous results (Wan et al., 2007). This finding indicates that porosity, rather than thickness of BC membranes, determines the extent of HAp deposition on fibrils inside BC membranes. It also suggests that BC should be cultured for at least 7 days when fully HAp-covered BC fibers are requested.

3.4. Structure of HAp deposited on BC cultured at different times

Fig. 8A presents XRD patterns of various BC/HAp samples obtained in this work. Notably, the characteristic peaks located at 14.8, 16.6, and 22.4° could be assigned to BC. In addition, there are two diffraction peaks detected at 25.9 and 31.7° which were due to the (0 0 2) and (2 1 1) crystal planes of HAp, respectively. Meanwhile, in these three patterns, the major peaks of HAp are broad and weak, indicating its poor crystallinity, consistent with our previous results (Wan et al., 2006). This XRD finding reveals that, although the BC templates were prepared under different lengths of culture time, no apparent difference was detected in the crystal structure of HAp among these BC/HAp nanocomposites.

The FTIR spectra of various BC/HAp samples are shown in Fig. 8B. It can be seen that the locations of characteristic peaks were consistent with each other and were identical to the FTIR spectra of BC/HAp reported in our previous work (Wan et al., 2006), indicating the chemical structure of these samples is identical even though the morphology of BC/HAp is changed with the culture time of BC templates.

4. Conclusions

The changes of morphology and structure of BC fiber network during the culture process starting from 0.5 h were assessed and HAp deposition on the obtained BC templates was investigated, upon which the feasibility of these BC pellicles as TE scaffolds was determined. It was found that porosity, fiber diameter, fiber network structure, light transmittance, and thickness of BC pellicles changed during the culture process while the surface and crystal structure of BC remained unchanged during the whole culture process. Furthermore, no difference was found in the crystal structure of HAp deposited on BC templates regardless of culture time. However, significant difference was observed in the distribution of HAp particles on the surface of nanofibers inside BC membranes due to the difference in the compactness of BC network. It was also found that a homogeneous integrated BC network was formed at 24-h incubation and a complete 3D porous network structure of BC was formed at day 5. In addition, homogeneous BC/HAp nanocomposites can be obtained as the culture time of BC templates reached 7 days. It can be concluded that the morphology of BC and BC/HAp scaffolds can be controlled by adjusting culture time to meet various TE requirement. The results presented in this work might help to select appropriate BC scaffolds for TE and proper BC templates for the deposition of HAp and other inorganics.

Acknowledgments

This work is supported by the National Natural Science Foundation of China (grant nos. 51172158 and 81200663) and the Science and Technology Support Program of Tianjin (grant no. 11ZCKFSY01700).

References

Andrade, F. K., Alexandre, N., Amorim, I., Gartner, F., Mauricio, A. C., Luis, A. L., & Gama, M. (2013). Studies on the biocompatibility of bacterial cellulose. *Journal of Bioactive and Compatible Polymers*, *28*(1), 97–112.

Barud, H. S., Assuncao, R. M. N., Martines, M. A. U., Dexpert-Ghys, J., Marques, R. F. C., Messaddeq, Y., & Ribeiro, S. J. L. (2008). Bacterial cellulose-silica organic-inorganic hybrids. *Journal of Sol–Gel Science and Technology*, *46*(3), 363–367.

Bashur, C. A., Dahlgren, L. A., & Goldstein, A. S. (2006). Effect of fiber diameter and orientation on fibroblast morphology and proliferation on electrospun poly(D,L-lactic-*co*-glycolic acid) meshes. *Biomaterials*, *27*(33), 5681–5688.

Beems, E. M., & Van Best, J. A. (1990). Light transmission of the cornea in whole human eyes. *Experimental Eye Research*, *50*(4), 393–395.

Berti, F. V., Rambo, C. R., Dias, P. F., & Porto, L. M. (2013). Nanofiber density determines endothelial cell behavior on hydrogel matrix. *Materials Science and Engineering C*, *33*(8), 4684–4691.

Berti, F. V., Recouvreux, D. O. S., Novikoff, S., Rambo, C. R., Dias, P. F., & Porto, L. M. (2011). Endothelization of artificial blood vessels inside large bodies of bacterial cellulose hydrogels. *International Journal of Artificial Organs*, *34*(8), 677–677.

Bhattarai, N., Edmondson, D., Veiseh, O., Matsen, F. A., & Zhang, M. Q. (2005). Electrospun chitosan-based nanofibers and their cellular compatibility. *Biomaterials*, *26*(31), 6176–6184.

Brown, R. M. (1987). The biosynthesis of cellulose. *Food Hydrocolloids*, *1*(5/6), 345–351.

Brown, R. M., Willison, J. H. M., & Richardson, C. L. (1976). Cellulose biosynthesis in *Acetobacter xylinum*: Visualization of the site of synthesis and direct measurement of the in vivo process. *Proceedings of the National academy of Sciences of the United States of America*, *73*, 4565–4569.

Chang, S. T., Chen, L. C., Lin, S. B., & Chen, H. H. (2012). Nano-biomaterials application: Morphology and physical properties of bacterial cellulose/gelatin composites via crosslinking. *Food Hydrocolloids*, *27*(1), 137–144.

Costa, S. V., Gonçalves, A. S., Zaghete, M. A., Mazon, T., & Nogueira, A. F. (2013). ZnO nanostructures directly grown on paper and bacterial cellulose substrates without any surface modification layer. *Chemical Communications*, *49*(73), 8096–8098.

Dugan, J. M., Gough, J. E., & Eichhorn, S. J. (2013). Bacterial cellulose scaffolds and cellulose nanowhiskers for tissue engineering. *Nanomedicine*, *8*(2), 287–298.

Fu, L., Zhang, Y., Li, C., Wu, Z., Zhuo, Q., Huang, X., Qiu, G., Zhou, P., & Yang, G. (2012). Skin tissue repair materials from bacterial cellulose by a multilayer fermentation method. *Journal of Materials Chemistry*, *22*(24), 12349–12357.

Fu, L., Zhou, P., Zhang, S., & Yang, G. (2013). Evaluation of bacterial nanocellulose-based uniform wound dressing for large area skin transplantation. *Materials Science and Engineering C*, *33*(5), 2995–3000.

Hong, L., Wang, Y. L., Jia, S. R., Huang, Y., Gao, C., & Wan, Y. Z. (2006). Hydroxyapatite/bacterial cellulose composites synthesized via a biomimetic route. *Materials Letters*, *60*(13–14), 1710–1713.

Iguchi, M., Yamanaka, S., & Budhiono, A. (2000). Bacterial cellulose—A masterpiece of nature's arts. *Journal of Materials Science*, *35*(2), 261–270.

Kim, D. Y., Nishiyama, Y., & Kuga, S. (2002). Surface acetylation of bacterial cellulose. *Cellulose*, *9*(3–4), 361–367.

Lin, W.-C., Lien, C.-C., Yeh, H.-J., Yu, C.-M., & Hsu, S.-H. (2013). Bacterial cellulose and bacterial cellulose–chitosan membranes for wound dressing applications. *Carbohydrate Polymers*, *94*(1), 603–611.

Liu, G., He, F., Li, X., Wang, S., Li, L., Zuo, G., Huang, Y., & Wan, Y. Z. (2011). Three-dimensional cuprous oxide microtube lattices with high catalytic activity templated by bacterial cellulose nanofibers. *Journal of Materials Chemistry*, *21*(29), 10637–10640.

Liu, X., Ma, Y., Zhou, Y., Pei, C., & Yin, G. (2013). A promising hybrid scaffold material: Bacterial cellulose in-situ assembling biomimetic lamellar $CaCO_3$. *Materials Letters*, *102*, 91–93.

Nge, T. T., Nogi, M., Yano, H., & Sugiyama, J. (2010). Microstructure and mechanical properties of bacterial cellulose/chitosan porous scaffold. *Cellulose*, *17*(2), 349–363.

Petersen, N., & Gatenholm, P. (2011). Bacterial cellulose-based materials and medical devices: Current state and perspectives. *Applied Microbiology and Biotechnology*, *91*(5), 1277–1286.

Ross, P., Mayer, R., & Benziman, M. (1991). Cellulose biosynthesis and function in bacteria. *Microbiology Review*, *55*(1), 35–58.

Saska, S., Teixeira, L. N., de Oliveira, P. T., Minarelli Gaspar, A. M., Lima Ribeiro, S. J., Messaddeq, Y., & Marchetto, R. (2012). Bacterial cellulose–collagen nanocomposite for bone tissue engineering. *Journal of Materials Chemistry*, *22*(41), 22102–22112.

Sheykhnazari, S., Tabarsa, T., Ashori, A., Shakeri, A., & Golalipour, M. (2011). Bacterial synthesized cellulose nanofibers; effects of growth times and culture mediums on the structural characteristics. *Carbohydrate Polymers*, *86*(3), 1187–1191.

Sionkowska, A., & Kozłowska, J. (2013). Properties and modification of porous 3-D collagen/hydroxyapatite composites. *International Journal of Biological Macromolecules*, *52*, 250–259.

Sottys, J., Lisowski, Z., & Knapczyk, J. (1984). X-ray diffraction study of the crystallinity index and the structure of the microcrystalline cellulose. *Acta Pharmaceutica Technologica*, *30*(2), 174–181.

Sundberg, J., Feldmann, E. M., Martinez, H., Schwarz, S., Rotter, N., & Gatenholm, P. (2012). Evaluation of macroporous bacterial nano-cellulose scaffolds for ear cartilage tissue engineering. *Journal of Tissue Engineering and Regenerative Medicine*, *6*, 153–153.

Svensson, A., Nicklasson, E., Harrah, T., Panilaitis, B., Kaplan, D. L., Brittberg, M., & Gatenholm, P. (2005). Bacterial cellulose as a potential scaffold for tissue engineering of cartilage. *Biomaterials*, *26*(4), 419–431.

Tang, W., Jia, S., Jia, Y., & Yang, H. (2010). The influence of fermentation conditions and post-treatment methods on porosity of bacterial cellulose membrane. *World Journal of Microbiology and Biotechnology*, *26*(1), 125–131.

Ul-Islam, M., Khan, T., Khattak, W. A., & Park, J. K. (2013). Bacterial cellulose-MMTs nanoreinforced composite films: Novel wound dressing material with antibacterial properties. *Cellulose*, *20*(2), 589–596.

Vandamme, E. J., De Baets, S., Vanbaelen, A., Joris, K., & De Wulf, P. (1998). Improved production of bacterial cellulose and its application potential. *Polymer Degradation and Stability*, *59*(1), 93–99.

Wan, Y. Z., Gao, C., Han, M., Liang, H., Ren, K., Wang, Y., & Luo, H. (2011). Preparation and characterization of bacterial cellulose/heparin hybrid nanofiber for potential vascular tissue engineering scaffolds. *Polymers for Advanced Technologies*, *22*(12), 2643–2648.

Wan, Y. Z., Hong, L., Jia, S. R., Huang, Y., Zhu, Y., Wang, Y. L., & Jiang, H. J. (2006). Synthesis and characterization of hydroxyapatite–bacterial cellulose nanocomposites. *Composites Science and Technology*, *66*(11), 1825–1832.

Wan, Y. Z., Huang, Y., Yuan, C. D., Raman, S., Zhu, Y., Jiang, H. J., He, F., & Gao, C. (2007). Biomimetic synthesis of hydroxyapatite/bacterial cellulose nanocomposites for biomedical applications. *Materials Science and Engineering C*, *27*(4), 855–864.

Wang, J., Gao, C., Zhang, Y., & Wan, Y. Z. (2010). Preparation and in vitro characterization of BC/PVA hydrogel composite for its potential use as artificial cornea biomaterial. *Materials Science and Engineering C*, *30*(1), 214–218.

Wang, J., Yang, C., Wan, Y. Z., Luo, H., He, F., Dai, K., & Huang, Y. (2013). Laser patterning of bacterial cellulose hydrogel and its modification with gelatin and hydroxyapatite for bone tissue engineering. *Soft Materials*, *11*(2), 173–180.

Watanabe, K., Tabuchi, M., Morinaga, Y., & Yoshinaga, F. (1998). Structural features and properties of bacterial cellulose produced in agitated culture. *Cellulose*, *5*(3), 187–200.

Yamanaka, S., Watanabe, K., Kitamura, N., Iguchi, M., Mitsuhashi, S., Nishi, Y., & Uryu, M. (1989). The structure and mechanical properties of sheets prepared from bacterial cellulose. *Journal of Materials Science*, *24*(9), 3141–3145.

Zhang, K. (2013). Illustration of the development of bacterial cellulose bundles/ribbons by Gluconacetobacter xylinus via atomic force microscopy. *Applied Microbiology and Biotechnology*, *97*(10), 4353–4359.